

# Adaptive Embedding for Temporal Network

Haoran Zhang and Junhui Wang

Department of Statistics  
The Chinese University of Hong Kong

## Abstract

Temporal network has become ubiquitous with the rise of online social platform and e-commerce, but largely under investigated in literature. In this paper, we propose a statistical framework for temporal network analysis, leveraging strengths of adaptive network merging, tensor decomposition and point process. A two-step embedding procedure and a regularized maximum likelihood estimate based on Poisson point process is developed, where the initial estimate is based on equal spaced time intervals while the final estimate on the adaptively merging time intervals. A projected gradient descent algorithm is proposed to facilitate estimation, where the upper bound of the tensor estimation error in each iteration is established. Through analysis, it is shown that the tensor estimation error is significantly reduced by the proposed method. Extensive numerical experiments also validate this phenomenon, as well as its advantage over other existing competitors. The proposed method is also applied to analyze a militarized interstate dispute dataset, where not only the prediction accuracy increases, but the adaptively merged intervals also lead to clear interpretation.

KEY WORDS: Continuous-time dynamic network, embedding, multi-layer network, point process, tensor decomposition

## 1 Introduction

Temporal network consists of a set of nodes and a sequence of temporal edges for each node pair, where the temporal edges may occur at different time (Holme and Saramäki, 2012). It provides a flexible framework to represent the time-varying network structure

and the evolution of pair-wise relationships. For example, in online social platform such as Facebook, users send likes to the posts of their friends recurrently at different time; in international politics, countries may conflict with others at one time but become allies at others. This is in sharp contrast to static network, and still frequently encountered in a wide spectrum of application domains, such as social science (Snijders, 2001; Perry-Smith and Shalley, 2003; Snijders et al., 2010), political science (Hays et al., 2010; Cranmer and Desmarais, 2011; Kinne, 2013), biological science (Sporns et al., 2004; Voytek and Knight, 2015; Avena-Koenigsberger et al., 2018) and ecological science (Ulanowicz, 2004; De Ruiter et al., 2005).

The primary goal of temporal network analysis is to model the network structure and how it evolves over time (Aggarwal and Subbian, 2014). One of the key challenges for temporal network analysis is that the edges are recorded on a continuous-time scale, where the interactions between nodes are instantaneous and come in a streaming fashion (Holme and Saramäki, 2012). This is the key difference from the discrete-time dynamic network (Kim et al., 2018), where snapshots of network are observed at a series of discrete time points. This also makes the models developed for dynamic network (Hanneke et al., 2010; Snijders, 2017; Matias and Miele, 2017; Sewell and Chen, 2015, 2016) inappropriate for temporal network analysis. Another common used approach for dynamic network is tensor factorization (Lyu et al., 2021; Han et al., 2022), where the discrete-time dynamic network is treated as an order-3 tensor with the first two dimensions representing the adjacency matrix and the third dimension the temporal evolution. However, such methods require relatively dense observations in each network slide, and may incur large estimation error in estimating the extremely sparse temporal network.

With the rapid rise of online social platform and e-commerce, novel methods for temporal network analysis are in demand. It was until recently that some attempts were made from the perspective of survival and event history analysis (Vu et al., 2011a,b; Perry and Wolfe,

2013; Sit et al., 2021), with a keen focus on inference of relationship between the temporal edge and some additional covariates. Another common practice is to merge the continuous-time temporal network into a multi-layer network based on a rather ad-hoc merging scheme (Huang et al., 2022), which may introduce unnecessary bias in network modeling.

In this paper, we propose a statistical framework for bipartite temporal network, leveraging strengths of adaptive network merging, tensor decomposition and point process. We first give a two-step embedding procedure. This initial step merges the dynamic network with some equally spaced small intervals, and estimate a low rank tensor by minimizing some distance measure. The second step adaptively merges adjacent small intervals with similar estimated temporal embedding vectors, and re-estimates the tensor based on the adaptively merged intervals. We further give a regularized maximum likelihood estimator based on Poisson point process whose intensity is determined by the out-node and in-node embedding vectors, as well as the temporal embedding vector at the specific time. A projected gradient descent algorithm is provided to facilitate estimation, and the tensor estimation error bound for each iteration is established. Through theoretical analysis, we find an interesting bias-variance tradeoff governed by the number of small intervals. Furthermore, the tensor estimation error, including the estimation bias and variance, is significantly reduced thanks to adaptively merging intervals. Extensive numerical experiments also validate this phenomenon, as well as its advantage over other existing competitors. Furthermore, the proposed method is also applied to analyze a militarized interstate dispute dataset, where not only the prediction accuracy increases, but the adaptively merged intervals also lead to clear interpretation.

The main contributions of this paper is summarized as follows. From the perspective of modeling, to the best of our limited knowledge, the proposed embedding model is the first structure-preserving model for temporal network, in sharp contrast to the existing methods that largely ignore the network structure but heavily rely on the additional covariates (Vu

et al., 2011a,b; Perry and Wolfe, 2013; Sit et al., 2021). Methodologically speaking, we develop a two-step embedding procedure for temporal network analysis, as well as a regularized maximum likelihood estimator. We also provide a projected gradient descent algorithm to maximize the non-convex regularized log likelihood, and establish the error bounds for each iteration without incurring the computational-statistical gap. Theoretically speaking, we formally prove that the proposed method based on the adaptively merged intervals could substantially reduce estimation error, compared with the commonly adopted approaches in literature based on the ad-hoc equally spaced intervals.

The rest of the paper is organized as follows. Section 2 first presents the two-step embedding procedure for temporal network, and then propose a regularized maximum likelihood estimator based on a temporal embedding model. Section 3 provides the details of the computation algorithm. Section 4 establishes the error bound for the proposed method. Numerical experiments on synthetic and real-life networks are contained in Section 5. Section 6 concludes the paper with a brief discussion, and technical proofs and necessary lemmas are provided in the Appendix.

**Notations.** Before moving to Section 2, we introduce some notations and preliminaries for tensor decomposition. For any  $n \geq r$ , let  $\mathbb{O}_{n,r} = \{\mathbf{U} \in \mathbb{R}^{n \times r} : \mathbf{U}^\top \mathbf{U} = \mathbf{I}_r\}$  and denote  $\mathbb{O}_r = \mathbb{O}_{r,r}$ . For a matrix  $\mathbf{U}$ , let  $\mathbf{U}_{[i]}$ ,  $\mathbf{U}_{[r]}$  and  $(\mathbf{U})_{ir}$  denote the  $i$ -th row,  $r$ -th column and element  $(i, r)$  of  $\mathbf{U}$ , respectively. Let  $\|\mathbf{U}\|_2$ ,  $\|\mathbf{U}\|_F$  denote its spectral and Frobenius norm, and  $\|\mathbf{U}\|_{2 \rightarrow \infty} = \max_i \|\mathbf{U}_{[i]}\|$ . For two matrix  $\mathbf{U}_1, \mathbf{U}_2 \in \mathbb{R}^{n \times r}$ , define the principal angle between them as

$$\sin \angle(\mathbf{U}_1, \mathbf{U}_2) = \max_{\mathbf{0} \neq \mathbf{u}_1 \in \text{span}(\mathbf{U}_1)} \min_{\mathbf{0} \neq \mathbf{u}_2 \in \text{span}(\mathbf{U}_2)} \sin \angle(\mathbf{u}_1, \mathbf{u}_2),$$

where  $\text{span}(\mathbf{U}_1)$  represent the column space of  $\mathbf{U}_1$ . For any order-3 tensor  $\mathcal{M} \in \mathbb{R}^{n_1 \times n_2 \times n_3}$ , let  $\mathcal{M}_{[i]}$ ,  $\mathcal{M}_{[j]}$ ,  $\mathcal{M}_{[k]}$  and  $(\mathcal{M})_{ijk}$  denote the  $i$ -th horizontal slides,  $j$ -th lateral slides,  $k$ -th

frontal slides and element  $(i, j, k)$  of  $\mathcal{M}$ , respectively. Let  $\Psi_k(\mathcal{M}) \in \mathbb{R}^{n_k \times n_{-k}}$  be the mode- $k$  unfolding of  $\mathcal{M}$ , where  $n_{-k} = n_1 n_2 n_3 / n_k$  for  $k = 1, 2, 3$ . We denote  $\text{rank}(\mathcal{M}) \leq (r_1, r_2, r_3)$  if  $\mathcal{M}$  admits the decomposition  $\mathcal{M} = \mathcal{S} \times_1 \mathbf{U} \times_2 \mathbf{V} \times_3 \mathbf{W} =: [\mathcal{S}; \mathbf{U}, \mathbf{V}, \mathbf{W}]$  for some  $\mathcal{S} \in \mathbb{R}^{r_1 \times r_2 \times r_3}$ ,  $\mathbf{U} \in \mathbb{R}^{n_1 \times r_1}$ ,  $\mathbf{V} \in \mathbb{R}^{n_2 \times r_2}$  and  $\mathbf{W} \in \mathbb{R}^{n_3 \times r_3}$ . For any order-3 tensor  $\mathcal{M}$  with  $\text{rank}(\mathcal{M}) \leq (r_1, r_2, r_3)$ , define

$$\begin{aligned}\bar{\lambda}(\mathcal{M}) &= \max \{ \|\Psi_1(\mathcal{M})\|_2, \|\Psi_2(\mathcal{M})\|_2, \|\Psi_3(\mathcal{M})\|_2 \}, \\ \underline{\lambda}(\mathcal{M}) &= \min \{ \sigma_{r_1}(\Psi_1(\mathcal{M})), \sigma_{r_2}(\Psi_2(\mathcal{M})), \sigma_{r_3}(\Psi_3(\mathcal{M})) \},\end{aligned}$$

where  $\sigma_r(\mathbf{M})$  denote the  $r$ -th largest singular value of matrix  $\mathbf{M}$ . Let  $\|\mathcal{M}\|_F = \sqrt{\sum_{i,j,k} m_{ijk}^2}$  be the Frobenius norm of  $\mathcal{M}$ . Throughout the paper, we use  $c, C, \epsilon$  and  $\kappa$  to denote positive constants whose values may vary according to context. For an integer  $m$ , let  $[m]$  denote the set  $\{1, \dots, m\}$ . For two nonnegative sequences  $a_{nT}$  and  $b_{nT}$ , where  $n$  and  $T$  are two subscripts, let  $a_{nT} \preceq b_{nT}$  and  $a_{nT} \prec b_{nT}$  denote  $a_{nT} = O(b_{nT})$  and  $a_{nT} = o(b_{nT})$ , respectively, as both  $n$  and  $T$  diverge. Denote  $a_{nT} \asymp b_{nT}$  if  $a_{nT} \preceq b_{nT}$  and  $b_{nT} \preceq a_{nT}$ . Further,  $a_{nT} \preceq_P b_{nT}$  means that there exists a positive constant  $c$  such that  $\Pr(a_{nT} \geq cb_{nT}) \rightarrow 0$  as  $(n, T)$  diverge.

## 2 Proposed method

Consider a bipartite temporal network  $\mathcal{G}_t = (\mathcal{N}_1, \mathcal{N}_2, \mathcal{E}_t)$  with  $t \in [0, T)$ , where  $\mathcal{N}_1$  and  $\mathcal{N}_2$  denote the groups of out-nodes and in-nodes with  $|\mathcal{N}_1| = n_1$  and  $|\mathcal{N}_2| = n_2$ , and  $\mathcal{E}_t$  consists of the directed edges  $e_{ij,t}$  pointing from out-node  $i \in \mathcal{N}_1$  to in-node  $j \in \mathcal{N}_2$  observed at time  $t$ . Suppose the edges in  $\mathcal{E}_t$  are generated from some distribution  $f(\Theta(t))$  with  $\Theta(t) = (\theta_{ij}(t))_{i,j=1}^n$ , which admits a low rank structure so that

$$\theta_{ij}(t) = \mathcal{S} \times_1 \mathbf{u}_i^\top \times_2 \mathbf{v}_j^\top \times_3 \mathbf{w}(t)^\top, \quad (1)$$

where  $\times_s$  denotes the mode- $s$  product for  $s \in [3]$ ,  $\mathcal{S} \in \mathbb{R}^{r_1 \times r_2 \times r_3}$  is an order-3 core tensor, and each out-node  $i$ , in-node  $j$  and time  $t$  are embedded as low-dimensional vectors  $\mathbf{u}_i \in \mathbb{R}^{r_1}$ ,  $\mathbf{v}_j \in \mathbb{R}^{r_2}$  and  $\mathbf{w}(t) \in \mathbb{R}^{r_3}$ , respectively. It is clear that the time-invariant network structure across all  $\mathcal{G}_t$ 's is captured by the network embedding vectors  $\mathbf{u}$  and  $\mathbf{v}$ , while the temporal structure in  $\mathcal{G}_t$ 's is captured by the temporal embedding vector  $\mathbf{w}(t)$ . Such a network embedding model has been widely employed for network data analysis (Hoff et al., 2002; Lyu et al., 2021; Zhang et al., 2022; Zhen and Wang, 2022), which embeds the unstructured network in a low-dimensional Euclidean space to facilitate the subsequent analysis.

## 2.1 Adaptive embedding

Note that the directed edges are observed in real time, which casts great challenge for embedding  $\mathcal{G}_t$  due to the fact that  $\mathcal{E}_t$  can be extremely sparse and may consist of only one observed edge. To circumvent the difficulty of severe under-sampling, we propose to embed the temporal network by adaptively merging  $\mathcal{G}_t$ 's into relatively dense networks based on their temporal structures, which produces a substantially improved embedding of the temporal network structure.

**Initial estimate.** We first split the time window  $[0, T)$  into  $L$  equally spaced small intervals with endpoints  $\{\delta_l\}_{l=1}^L$ , where  $\delta_l = l\Delta_\delta$ ,  $\delta_0 = 0$ , and each interval  $[\delta_{l-1}, \delta_l)$  is of width  $\Delta_\delta = T/L$ . When  $\Delta_\delta$  is sufficiently small, it is generally believed that  $\Theta(t)$  shall be roughly constant within each time interval. As a direct consequence,  $\Theta(t)$  can be estimated by a low rank order-3 tensor  $\mathcal{M} \in \mathbb{R}^{n_1 \times n_2 \times L}$ , which admits a Tucker decomposition with rank  $(r_1, r_2, r_3)$ ,

$$\mathcal{M} = \mathcal{S} \times_1 \mathbf{U} \times_2 \mathbf{V} \times_3 \mathbf{W},$$

with  $\mathbf{u}_i, \mathbf{v}_j$  and  $\mathbf{w}_l$  being the corresponding rows of  $\mathbf{U}, \mathbf{V}$  and  $\mathbf{W}$ , respectively. Let  $\boldsymbol{\delta} = (\delta_1, \dots, \delta_L)^\top$  and  $\mathcal{Y}_\delta \in \mathbb{R}^{n_1 \times n_2 \times L}$  with  $(\mathcal{Y}_\delta)_{ijl} = |\mathcal{T}_{ij} \cap [\delta_{l-1}, \delta_l)|$  representing the number of

temporal edges in each small interval. An initial estimate  $(\widehat{\mathcal{S}}_\delta, \widehat{\mathbf{U}}_\delta, \widehat{\mathbf{V}}_\delta, \widehat{\mathbf{W}}_\delta)$  can be obtained by minimizing certain distance measure between  $\mathcal{M}$  and  $\mathcal{Y}_\delta$ , to be specified in Section 2.2.

**Improved estimate via adaptive embedding.** Once we obtain the initial estimate  $\widehat{\mathbf{W}}_\delta = (\widehat{\mathbf{w}}_{1,\delta}, \dots, \widehat{\mathbf{w}}_{L,\delta})^\top$ , define

$$\widetilde{\mathbf{W}}_\delta = (\widetilde{\mathbf{w}}_{1,\delta}, \dots, \widetilde{\mathbf{w}}_{L,\delta})^\top = \sqrt{L} \widehat{\mathbf{W}}_\delta ((\widehat{\mathbf{W}}_\delta)^\top \widehat{\mathbf{W}}_\delta)^{-\frac{1}{2}},$$

where  $(\widehat{\mathbf{W}}_\delta)^\top \widehat{\mathbf{W}}_\delta$  is invertible with high probability as to be showed in the proof of Theorem 2. Though consistent, the estimation variance of  $\widehat{\mathbf{W}}_\delta$  can be exceedingly large when  $\Delta_\delta$  is too small. We then propose to merge adjacent small intervals with similar temporal embedding vectors  $\widetilde{\mathbf{w}}_{l,\delta}$ , so as to shrink the estimation variance without compromising the estimation bias.

To this end, define  $\mathcal{P} = \{\mathcal{P}_1, \dots, \mathcal{P}_K\}$  as an ordered partition of  $\{1, \dots, L\}$ , where for any  $l_1 \in \mathcal{P}_{k_1}$  and  $l_2 \in \mathcal{P}_{k_2}$ , it holds that  $l_1 < l_2$  if  $k_1 < k_2$ . Here  $K$  is the number of merged intervals which will be specified in Section 3. Then, the ordered partition can be estimated as

$$\widehat{\mathcal{P}} = \arg \min_{\mathcal{P}} \sum_{k=1}^K \sum_{l \in \mathcal{P}_k} \|\widetilde{\mathbf{w}}_{l,\delta} - \boldsymbol{\mu}_k\|^2, \quad (2)$$

where  $\boldsymbol{\mu}_k = |\mathcal{P}_k|^{-1} \sum_{l \in \mathcal{P}_k} \widetilde{\mathbf{w}}_{l,\delta}$ . Note that (2) is equivalent to seeking change points in the sequence  $(\widetilde{\mathbf{w}}_{1,\delta}, \dots, \widetilde{\mathbf{w}}_{L,\delta})$ , and thus can be efficiently solved by multiple change point detection algorithm (Hao et al., 2013; Niu et al., 2016). Further, define  $\widehat{\eta}_k = \Delta_\delta \max \widehat{\mathcal{P}}_k$ , and thus  $\widehat{\boldsymbol{\eta}} = (\widehat{\eta}_1, \dots, \widehat{\eta}_K)^\top$  consists of the estimated endpoints of  $K$  adaptively merged intervals. Denote  $\mathcal{Y}_{\widehat{\boldsymbol{\eta}}} \in \mathbb{R}^{n_1 \times n_2 \times K}$  with  $(\mathcal{Y}_{\widehat{\boldsymbol{\eta}}})_{ijk} = |\mathcal{T}_{ij} \cap [\widehat{\eta}_{k-1}, \widehat{\eta}_k]|$  with  $\widehat{\eta}_0 = 0$ , the final estimate  $(\widehat{\mathcal{S}}_{\widehat{\boldsymbol{\eta}}}, \widehat{\mathbf{U}}_{\widehat{\boldsymbol{\eta}}}, \widehat{\mathbf{V}}_{\widehat{\boldsymbol{\eta}}}, \widehat{\mathbf{W}}_{\widehat{\boldsymbol{\eta}}})$  is then obtained by minimizing the distance measure between  $\mathcal{M}$  and  $\mathcal{Y}_{\widehat{\boldsymbol{\eta}}}$ .

## 2.2 Poisson point process

To devise a proper distance measure, let  $y_{ij}(\cdot)$  be the point process that counts the number of directed edges out-node  $i$  sends to in-node  $j$  during  $[0, T)$ . Particularly, out-node  $i$  sends a directed edge to in-node  $j$  at time  $t$  if and only if  $dy_{ij}(t) = 1$ . Given  $\Theta(t) = (\theta_{ij}(t))_{n_1 \times n_2}$ , we assume that  $y_{ij}(\cdot)$ 's are mutually independent Poisson processes such that

$$\mathbb{E}(dy_{ij}(t) \mid \theta_{ij}(t)) = \lambda_0 e^{\theta_{ij}(t)} dt \quad (3)$$

where  $\theta_{ij}(t)$  is the underlying propensity for node pair  $(i, j)$  at time  $t$ , and  $\lambda_0 > 0$  is the baseline intensity. The larger  $\theta_{ij}(t)$  is, the more likely out-node  $i$  will send a directed edge to in-node  $j$  during  $[t, t + dt)$ . The log-likelihood function of  $\{y_{ij}(t)\}_{1 \leq i \leq n_1, 1 \leq j \leq n_2}$  can become

$$l(\Theta) = \sum_{i=1}^{n_1} \sum_{j=1}^{n_2} \left\{ \sum_{t \in \mathcal{T}_{ij}} \log \lambda_{ij}(t) - \int_0^T \lambda_{ij}(s) ds \right\}, \quad (4)$$

where  $\lambda_{ij}(t) = \lambda_0 \exp(\theta_{ij}(t))$ . Note that  $\lambda_0$  is fixed throughout the paper, but it could also be varying with  $t$ , which may require more involved treatment.

Let  $\boldsymbol{\tau} = (\tau_0, \dots, \tau_{n_3})^T$  denote a generic partition of  $[0, T)$  with  $0 = \tau_0 < \tau_1 < \dots < \tau_{n_3} = T$ . Particularly,  $\boldsymbol{\tau}$  could be the equally spaced intervals  $\boldsymbol{\delta}$  for the initial estimate or the adaptively merged intervals  $\widehat{\boldsymbol{\eta}}$  for the final estimate in Section 2.1, and  $n_3$  could be  $L$  or  $K$ , correspondingly. For any  $\mathcal{M} \in \mathbb{R}^{n_1 \times n_2 \times n_3}$ , we define

$$l(\mathcal{M}; \boldsymbol{\tau}) = \sum_{i=1}^{n_1} \sum_{j=1}^{n_2} \sum_{l=1}^{n_3} \{m_{ijl} \mid \mathcal{T}_{ij} \cap [\tau_{l-1}, \tau_l) \mid - e^{m_{ijl}} \lambda_0 (\tau_l - \tau_{l-1})\}. \quad (5)$$

Note that if  $\Theta(t)$  is roughly constant in each interval, we consider the regularized formulation,

$$(\widehat{\mathcal{S}}_{\boldsymbol{\tau}}, \widehat{\mathbf{U}}_{\boldsymbol{\tau}}, \widehat{\mathbf{V}}_{\boldsymbol{\tau}}, \widehat{\mathbf{W}}_{\boldsymbol{\tau}}) = \arg \min_{\mathcal{S}, \mathbf{U}, \mathbf{V}, \mathbf{W}} \{-l(\mathcal{M}; \boldsymbol{\tau}) + \gamma_{\boldsymbol{\tau}} \mathcal{J}_{\boldsymbol{\tau}}(\mathbf{U}, \mathbf{V}, \mathbf{W})\}, \quad (6)$$



where  $\gamma_\tau$  is the tuning parameter,  $\mathcal{J}_\tau(\mathbf{U}, \mathbf{V}, \mathbf{W})$  is the regularization term which takes the form

$$\mathcal{J}_\tau(\mathbf{U}, \mathbf{V}, \mathbf{W}) = \frac{1}{4} \left\{ \left\| \frac{1}{n_1} \mathbf{U}^\top \mathbf{U} - \mathbf{I}_{r_1} \right\|_F^2 + \left\| \frac{1}{n_2} \mathbf{V}^\top \mathbf{V} - \mathbf{I}_{r_2} \right\|_F^2 + \left\| \frac{1}{n_3} \mathbf{W}^\top \mathbf{W} - \mathbf{I}_{r_3} \right\|_F^2 \right\},$$

encouraging the orthogonality among columns in  $\mathbf{U}, \mathbf{V}$  and  $\mathbf{W}$ . A similar regularization term has also been employed in Han et al. (2022), which involves some additional tuning parameter and thus requires more computational efforts.

### 3 Computation

Define  $\mathcal{C}_\mathcal{S} = \{\mathcal{S} \in \mathbb{R}^{r_1 \times r_2 \times r_3} : \|\mathcal{S}\|_F \leq c_\mathcal{S}\}$ ,  $\mathcal{C}_\mathbf{U} = \{\mathbf{U} \in \mathbb{R}^{n_1 \times r_1} : \|\mathbf{U}\|_{2 \rightarrow \infty} \leq c_\mathbf{U}\}$ ,  $\mathcal{C}_\mathbf{V} = \{\mathbf{V} \in \mathbb{R}^{n_2 \times r_2} : \|\mathbf{V}\|_{2 \rightarrow \infty} \leq c_\mathbf{V}\}$ , and  $\mathcal{C}_{\mathbf{W}, \delta} = \{\mathbf{W} \in \mathbb{R}^{L \times r_3} : \|\mathbf{W}\|_{2 \rightarrow \infty} \leq c_\mathbf{W}\}$ , where  $c_\mathcal{S}, c_\mathbf{U}, c_\mathbf{V}$  and  $c_\mathbf{W}$  are constants. Let

$$\mathcal{C}_{\mathcal{M}, \delta} = \{\mathcal{M} = [\mathcal{S}; \mathbf{U}, \mathbf{V}, \mathbf{W}] : \mathcal{S} \in \mathcal{C}_\mathcal{S}, \mathbf{U} \in \mathcal{C}_\mathbf{U}, \mathbf{V} \in \mathcal{C}_\mathbf{V}, \mathbf{W} \in \mathcal{C}_{\mathbf{W}, \delta}\}.$$

Further define  $\mathcal{C}_{\mathbf{W}, \eta} = \{\mathbf{W} \in \mathbb{R}^{K \times r_3} : \|\mathbf{W}\|_{2 \rightarrow \infty} \leq c_\mathbf{W}\}$  and

$$\mathcal{C}_{\mathcal{M}, \eta} = \{\mathcal{M} = [\mathcal{S}; \mathbf{U}, \mathbf{V}, \mathbf{W}] : \mathcal{S} \in \mathcal{C}_\mathcal{S}, \mathbf{U} \in \mathcal{C}_\mathbf{U}, \mathbf{V} \in \mathcal{C}_\mathbf{V}, \mathbf{W} \in \mathcal{C}_{\mathbf{W}, \eta}\}.$$

For any convex set  $\mathcal{C}$ , denote  $\mathcal{P}_\mathcal{C}$  to be the projection operator onto  $\mathcal{C}$ .

We develop an efficient projected gradient updating algorithm to solve the optimization task in (6). Choose an initializer  $(\mathcal{S}_\tau^{(0)}, \mathbf{U}_\tau^{(0)}, \mathbf{V}_\tau^{(0)}, \mathbf{W}_\tau^{(0)})$  such that  $\mathcal{S}_\tau^{(0)} \in \mathcal{C}_\mathcal{S}$ ,  $\mathbf{U}_\tau^{(0)} \in \mathcal{C}_\mathbf{U}$ ,  $\mathbf{V}_\tau^{(0)} \in \mathcal{C}_\mathbf{V}$  and  $\mathbf{W}_\tau^{(0)} \in \mathcal{C}_{\mathbf{W}, \tau}$ , with  $\mathbf{U}_\tau^{(0)\top} \mathbf{U}_\tau^{(0)} = n_1 \mathbf{I}_{r_1}$ ,  $\mathbf{V}_\tau^{(0)\top} \mathbf{V}_\tau^{(0)} = n_2 \mathbf{I}_{r_2}$  and  $\mathbf{W}_\tau^{(0)\top} \mathbf{W}_\tau^{(0)} = n_3 \mathbf{I}_{r_3}$ . Given  $(\mathcal{S}_\tau^{(r)}, \mathbf{U}_\tau^{(r)}, \mathbf{V}_\tau^{(r)}, \mathbf{W}_\tau^{(r)})$  and  $\mathcal{M}_\tau^{(r)} = [\mathcal{S}_\tau^{(r)}; \mathbf{U}_\tau^{(r)}, \mathbf{V}_\tau^{(r)}, \mathbf{W}_\tau^{(r)}]$ , we implement the

following updating scheme with step size  $\zeta_\tau$ :

$$\begin{aligned}
\mathbf{U}_\tau^{(r+1)} &= \mathcal{P}_{\mathcal{C}_U} \left\{ \mathbf{U}_\tau^{(r)} + \zeta_\tau \left[ n_1 \frac{\partial l(\mathcal{M}_\tau^{(r)}; \boldsymbol{\tau})}{\partial \mathbf{U}} - \gamma_\tau \mathbf{U}_\tau^{(r)} \left( \frac{1}{n_1} \mathbf{U}_\tau^{(r)\top} \mathbf{U}_\tau^{(r)} - \mathbf{I}_{r_1} \right) \right] \right\}; \\
\mathbf{V}_\tau^{(r+1)} &= \mathcal{P}_{\mathcal{C}_V} \left\{ \mathbf{V}_\tau^{(r)} + \zeta_\tau \left[ n_2 \frac{\partial l(\mathcal{M}_\tau^{(r)}; \boldsymbol{\tau})}{\partial \mathbf{V}} - \gamma_\tau \mathbf{V}_\tau^{(r)} \left( \frac{1}{n_2} \mathbf{V}_\tau^{(r)\top} \mathbf{V}_\tau^{(r)} - \mathbf{I}_{r_2} \right) \right] \right\}; \\
\mathbf{W}_\tau^{(r+1)} &= \mathcal{P}_{\mathcal{C}_{\mathbf{W}, \tau}} \left\{ \mathbf{W}_\tau^{(r)} + \zeta_\tau \left[ n_3 \frac{\partial l(\mathcal{M}_\tau^{(r)}; \boldsymbol{\tau})}{\partial \mathbf{W}} - \gamma_\tau \mathbf{W}_\tau^{(r)} \left( \frac{1}{n_3} \mathbf{W}_\tau^{(r)\top} \mathbf{W}_\tau^{(r)} - \mathbf{I}_{r_3} \right) \right] \right\}; \\
\mathcal{S}_\tau^{(r+1)} &= \mathcal{P}_{\mathcal{C}_S} \left\{ \mathcal{S}_\tau^{(r)} + \zeta_\tau \frac{\partial l(\mathcal{M}_\tau^{(r)}; \boldsymbol{\tau})}{\partial \mathcal{S}} \right\},
\end{aligned} \tag{7}$$

and let  $\mathcal{M}_\tau^{(r+1)} = [\mathcal{S}_\tau^{(r+1)}; \mathbf{U}_\tau^{(r+1)}, \mathbf{V}_\tau^{(r+1)}, \mathbf{W}_\tau^{(r+1)}]$ . We repeat the above updating scheme for a relative large number of iterations, say  $R$ , and let  $(\widehat{\mathcal{S}}_\tau, \widehat{\mathbf{U}}_\tau, \widehat{\mathbf{V}}_\tau, \widehat{\mathbf{W}}_\tau) = (\mathcal{S}_\tau^{(R)}, \mathbf{U}_\tau^{(R)}, \mathbf{V}_\tau^{(R)}, \mathbf{W}_\tau^{(R)})$  be the initial estimation.

**Remark 1.** We point out that the updating scheme in (7) differs from the standard projected gradient descent update, as different step sizes are used for updating different variables. Specifically, the step sizes for updating  $\mathbf{U}_\tau^{(r)}, \mathbf{V}_\tau^{(r)}, \mathbf{W}_\tau^{(r)}, \mathcal{S}_\tau^{(r)}$  are  $n_1\zeta_\tau, n_2\zeta_\tau, n_3\zeta_\tau$  and  $\zeta_\tau$ , respectively. This is the key difference from the algorithm in Han et al. (2022), which is also the reason that we do not require additional tuning parameter in  $\mathcal{J}_\tau(\mathbf{U}, \mathbf{V}, \mathbf{W})$  and  $\mathcal{J}_\eta(\mathbf{U}, \mathbf{V}, \mathbf{W})$ .

It remains to determine the number of merged interval  $K$  in (2), which differs from estimating the number of change points in  $(\widetilde{\mathbf{w}}_{1,\delta}, \dots, \widetilde{\mathbf{w}}_{L,\delta})$ , since  $\widetilde{\mathbf{w}}_{1,\delta}, \dots, \widetilde{\mathbf{w}}_{L,\delta}$  are dependent with each other. In particular, we set

$$\widehat{K} = \arg \min_S \left\{ \min_{\mathcal{P}} \mathcal{L}(\mathcal{P}; S) + \nu_{nT} S \right\}, \tag{8}$$

where  $\mathcal{P} = \{\mathcal{P}_1, \dots, \mathcal{P}_S\}$  is an ordered partition of  $[L]$  with  $S$  subsets,  $\nu_{nT}$  is a quantity to be

specified in Theorem 2 and Remark 3, and

$$\mathcal{L}(\mathcal{P}; S) = \frac{1}{L} \sum_{s=1}^S \sum_{l \in \mathcal{P}_s} \|\tilde{\mathbf{w}}_{l,\delta} - \boldsymbol{\mu}_s\|^2, \quad (9)$$

with  $\boldsymbol{\mu}_s = |\mathcal{P}_s|^{-1} \sum_{l \in \mathcal{P}_s} \tilde{\mathbf{w}}_{l,\delta}$ . More importantly,  $\hat{K}$  can be showed to be a consistent estimator of  $K$  under mild conditions as in Theorem 2.

## 4 Theory

Suppose  $c^{-1} \leq n_1/n_2 \leq c$  for a constant  $c$ , and let  $n = \max\{n_1, n_2\}$  for simplicity. We consider the asymptotic regime that both  $n$  and  $T$  grow to infinity. Suppose the temporal network  $\mathcal{G}_t$  is generated with  $\Theta^*(t) = \mathcal{S}^* \times_1 \mathbf{U}^* \times_2 \mathbf{V}^* \times_3 \mathbf{w}^*(t)$ , where  $\text{rank}(\Psi_s(\mathcal{S}^*)) = r_s$  for  $s = 1, 2, 3$ ,  $\mathbf{U}^{*\top} \mathbf{U}^* = n_1 \mathbf{I}_{r_1}$ ,  $\mathbf{V}^{*\top} \mathbf{V}^* = n_2 \mathbf{I}_{r_2}$  and  $\int_0^T \mathbf{w}^*(t) \mathbf{w}^*(t)^\top dt = T \mathbf{I}_{r_3}$ . Further, suppose  $\mathbf{w}^*(t)$  is a piecewise constant function of  $t$  in that  $\mathbf{w}^*(t) = \mathbf{w}_{k,\boldsymbol{\eta}}^*$  for  $t \in [\eta_{k-1}, \eta_k)$ , where  $\boldsymbol{\eta} = (\eta_1, \dots, \eta_{K_0})^\top$  with  $0 = \eta_0 < \eta_1 < \dots < \eta_{K_0} = T$ . Denote  $d_{\min} = \min_{1 \leq k \leq K_0} (\eta_k - \eta_{k-1})/T$ ,  $d_{\max} = \max_{1 \leq k \leq K_0} (\eta_k - \eta_{k-1})/T$ , and  $\Delta_{\boldsymbol{\eta}} = \min_{1 \leq k \leq K_0} (\eta_k - \eta_{k-1})$ . Suppose  $d_{\min} \asymp d_{\max} \asymp 1/K_0$ ,  $\|\mathcal{S}^*\|_F \leq c_S / \max\{2, (K_0 d_{\min})^{-1/2}\}$ ,  $\|\mathbf{U}^*\|_{2 \rightarrow \infty} \leq c_{\mathbf{U}}$ ,  $\|\mathbf{V}^*\|_{2 \rightarrow \infty} \leq c_{\mathbf{V}}$  and  $\sup_{t \in [0, T)} \|\mathbf{w}^*(t)\| \leq c_{\mathbf{w}} / \max\{2, \sqrt{K_0 d_{\max}}\}$ . Further, let  $\mathbf{W}_{\boldsymbol{\eta}}^* \in \mathbb{R}^{K_0 \times r_3}$  with  $(\mathbf{W}_{\boldsymbol{\eta}}^*)_{[k, \cdot]} = \mathbf{w}_{k,\boldsymbol{\eta}}^*$ , and  $\mathcal{M}_{\boldsymbol{\eta}}^* = [\mathcal{S}^*; \mathbf{U}^*, \mathbf{V}^*, \mathbf{W}_{\boldsymbol{\eta}}^*]$ .

Let  $p = \Delta_{\boldsymbol{\eta}}/T$  be the proportion of each small interval relative to  $[0, T)$ , and suppose  $K_0 p \prec 1$ . The following Theorem 1 establishes the tensor error bound for the initial estimate based on equal spaced interval  $\boldsymbol{\delta}$ .

**Theorem 1. (Initial estimate)** *Suppose  $\gamma_{\boldsymbol{\delta}} \asymp n^2 L \Delta_{\boldsymbol{\delta}}$ . Then, there exists a constant  $c_0 > 0$  such that for a step size  $\zeta_{\boldsymbol{\delta}} = \frac{c}{n^2 L \Delta_{\boldsymbol{\delta}}}$  with  $0 < c < c_0$ , with probability approaching 1, it holds true that*

$$\frac{1}{n_1 n_2 L} \|\mathcal{M}_{\boldsymbol{\delta}}^{(R)} - \mathcal{M}_{\boldsymbol{\delta}}^*\|_F^2 \preceq I_{1,\boldsymbol{\delta}} + I_{2,\boldsymbol{\delta}} + I_{3,\boldsymbol{\delta}},$$

where  $\mathcal{M}_\delta^* = [\mathcal{S}^*; \mathbf{U}^*, \mathbf{V}^*, \mathbf{W}_\delta^*]$  with  $\mathbf{W}_\delta^* \in \mathbb{R}^{L \times r_3}$  such that  $(\mathbf{W}_\delta^*)_{[l,]} = \mathbf{w}^*(\delta_{l-1})$ . Here

$$I_{1,\delta} = \begin{cases} \frac{1}{nT} + \frac{1}{n^2Tp}, & \text{if } p \succ \frac{\log(n/p)}{T}, \\ \frac{\log(n/p)^2}{T^2p} + \frac{\log(n/p)^2}{n^2T^2p^3}, & \text{if } \max \left\{ \frac{\log(n/p)^2}{T^2}, \left( \frac{\log(n/p)}{nT} \right)^{\frac{2}{3}} \right\} \preceq p \preceq \frac{\log(n/p)}{T}, \end{cases}$$

$I_{2,\delta} = K_0p$  and  $I_{3,\delta} = C(1 - \kappa)^R$  for some constants  $C$  and  $0 < \kappa < 1$ .

Respectively,  $I_{1,\delta}$ ,  $I_{2,\delta}$  and  $I_{3,\delta}$  correspond to the estimation variance, the bias induced by the partition, and the computational error of (7) after  $R$  iterations. The trade-off among these three terms largely determines the convergence rate of  $\|\mathcal{M}_\delta^{(R)} - \mathcal{M}_\delta^*\|_F^2$ . In the sequel, we take a relatively large value of  $R$ , so that  $I_{3,\delta}$  is dominated by  $I_{1,\delta} + I_{2,\delta}$ .

**Remark 2.** We discuss the convergence rate under different scenarios with different choice of  $p$ , where the logarithmic factor is suppressed to simplify the discussion.

1. If  $T \preceq n$ , then  $I_{1,\delta} + I_{2,\delta} \asymp \frac{\sqrt{K_0}}{T}$  with  $p \asymp \frac{1}{T\sqrt{K_0}}$ ;
2. if  $n \prec T \preceq n\sqrt{K_0}$ , then  $I_{1,\delta} + I_{2,\delta} \asymp \frac{K_0^{\frac{3}{4}}}{\sqrt{nT}}$  with  $p \asymp \frac{1}{\sqrt{nTK_0^{\frac{1}{4}}}}$ ;
3. if  $n\sqrt{K_0} \prec T \preceq n^2K_0$ , then  $I_{1,\delta} + I_{2,\delta} \asymp \frac{K_0}{T}$  with  $p \asymp \frac{1}{T}$ ;
4. if  $T \succ n^2K_0$ , then  $I_{1,\delta} + I_{2,\delta} \asymp \frac{\sqrt{K_0}}{n\sqrt{T}}$  with  $p \asymp \frac{1}{n\sqrt{K_0T}}$ .

It could be seen that when  $T \succ n\sqrt{K_0}$ , the optimal convergence rate is obtained with  $p \succ 1/T$ . In contrast, when  $T \preceq n\sqrt{K_0}$ , the optimal convergence rate is obtained with  $p \preceq 1/T$ . It is interesting to point out that the results for Poisson tensor PCA in Han et al. (2022) and Cai et al. (2022) only consider the case under strong intensity assumption, which are not applicable to the case when  $p \preceq 1/T$ . We should also point out that  $p$  could not be chosen too small; otherwise there are too few edges observed in each interval  $[\delta_{l-1}, \delta_l)$  leading to a large estimation variance  $I_{1,\delta} \succeq 1$ .

Define  $\rho = \min_{k \in [K_0]} \|\mathbf{w}_{k,\boldsymbol{\eta}}^* - \mathbf{w}_{k-1,\boldsymbol{\eta}}^*\|$  and suppose  $\rho \succeq 1$ . Denote  $r_{nT} = I_{1,\delta} + I_{2,\delta}$  as the upper bound in Theorem 1. Theorem 2 shows that (8) gives a consistent estimate of  $K_0$ , and (2) further results in a precise recovery of the true partition  $\boldsymbol{\eta}$  with overwhelming probability.

**Theorem 2. (Consistency of partition)** *Suppose the conditions of Theorem 1 are satisfied, and  $r_{nT} \prec \nu_{nT} \prec 1/K_0$ . Then as  $n$  and  $T$  grow to infinity, we have  $\Pr(\widehat{K} = K_0) \rightarrow 1$  and  $\|\widehat{\boldsymbol{\eta}} - \boldsymbol{\eta}\|_\infty \preceq_P T r_{nT}$ .*

**Remark 3.** *It is clear that the consistency of  $\widehat{K}$  is guaranteed with a wide range of  $\nu_{nT}$ . Specifically, the condition  $\nu_{nT} \prec 1/K_0$  implies that  $\widehat{K} \geq K_0$ , whereas  $\nu_{nT} \succ r_{nT}$  guarantees  $\widehat{K} \leq K_0$ . More importantly, Theorem 2 and Remark 2 provide valuable guidelines for choosing  $p$  and  $\nu_{nT}$ . For instance, if  $K_0$  is fixed, we have the following choices of  $p$  and  $\nu_{nT}$ : (1) if  $T \preceq n^2$ , we choose  $p \asymp 1/T$  and  $\nu_{nT} = 1/\sqrt{T}$ ; (2) if  $T \succ n^2$ , we choose  $p \asymp 1/(n\sqrt{T})$  and  $\nu_{nT} = 1/(\sqrt{n}T^{1/4})$ , where the logarithmic factor is also suppressed for simplicity.*

Given that the true partition  $\boldsymbol{\eta}$  is accurately estimated by  $\widehat{\boldsymbol{\eta}}$ , Theorem 3 further shows that estimation based on the adaptively merged intervals can attain a faster rate of convergence than that in Theorem 1.

**Theorem 3. (Improved estimate via adaptive embedding)** *Suppose the conditions of Theorem 2 are satisfied,  $K_0 r_{nT} \prec 1$ ,  $T \succeq K_0 \log(nK_0)$  and  $\gamma_\boldsymbol{\eta} \asymp n^2 K_0 \Delta_\boldsymbol{\eta}$ . Then, there exists  $c_0 > 0$  such that for a step size  $\zeta_\boldsymbol{\eta} = \frac{c}{n^2 K_0 \Delta_\boldsymbol{\eta}}$  with  $0 < c < c_0$ , with probability approaching 1, we have*

$$\frac{1}{n_1 n_2 K_0} \|\mathcal{M}_{\widehat{\boldsymbol{\eta}}}^{(R)} - \mathcal{M}_{\boldsymbol{\eta}}^*\|_F^2 \preceq I_{1,\boldsymbol{\eta}} + I_{2,\boldsymbol{\eta}} + I_{3,\boldsymbol{\eta}},$$

where  $I_{1,\boldsymbol{\eta}} = \frac{1}{nT} + \frac{K_0}{n^2 T}$ ,  $I_{2,\boldsymbol{\eta}} = K_0^2 r_{nT}^2$  and  $I_{3,\boldsymbol{\eta}} = C(1 - \kappa)^r$  for some constants  $C$  and  $0 < \kappa < 1$ .

Similarly,  $I_{1,\boldsymbol{\eta}}$ ,  $I_{2,\boldsymbol{\eta}}$  and  $I_{3,\boldsymbol{\eta}}$  correspond to the estimation variance, the bias induced by the initial estimation and computational error of (7) after  $R$  iterations, respectively. It is

clear that  $I_{1,\eta} + I_{2,\eta}$  is smaller than  $I_{1,\delta} + I_{2,\delta}$  in Theorem 1, suggesting the great advantage of adaptively merged intervals. Specifically, the variance term  $K_0/(n^2T)$  is clearly smaller than  $1/(n^2Tp) = L/(n^2T)$  in  $I_{1,\delta}$ , and the bias term  $I_{2,\eta} = K_0^2 r_{nT}^2 \asymp \max(I_{1,\delta}^2, I_{2,\delta}^2)$ .

**Corollary 1. (Consistency of embedding)** *Suppose the conditions of Theorem 3 are satisfied. With probability approaching 1, we have*

$$\begin{aligned} \max \left\{ \sin \angle(\widehat{\mathbf{U}}_\delta, \mathbf{U}^*), \sin \angle(\widehat{\mathbf{V}}_\delta, \mathbf{V}^*) \right\} &\preceq \sqrt{I_{1,\delta} + I_{2,\delta} + I_{3,\delta}}, \\ \max \left\{ \sin \angle(\widehat{\mathbf{U}}_\eta, \mathbf{U}^*), \sin \angle(\widehat{\mathbf{V}}_\eta, \mathbf{V}^*) \right\} &\preceq \sqrt{I_{1,\eta} + I_{2,\eta} + I_{3,\eta}}. \end{aligned}$$

Corollary 1 states that the true embedding vectors  $(\mathbf{U}^*, \mathbf{V}^*)$  can be consistently estimated by both  $(\widehat{\mathbf{U}}_\delta, \widehat{\mathbf{V}}_\delta)$  and  $(\widehat{\mathbf{U}}_\eta, \widehat{\mathbf{V}}_\eta)$ . More importantly, the estimation error of  $(\widehat{\mathbf{U}}_\eta, \widehat{\mathbf{V}}_\eta)$  is also substantially reduced thanks to the adaptively merging intervals. This implies that the proposed method yields more accurate estimates of the node embedding vectors, and thus shall greatly benefit the subsequent analysis, such as community detection and node classification.

## 5 Numerical experiments

### 5.1 Simulation examples

We investigate the finite-sample performance of the proposed method, and compare it with a number of existing tensor decomposition methods, including a modified Poisson tensor PCA (Han et al., 2022), higher-order SVD (De Lathauwer et al., 2000a) and higher-order orthogonal iteration (De Lathauwer et al., 2000b). We denote them as  $\text{AM}(\widehat{K})$ ,  $\text{ES}(L)$ ,  $\text{HOSVD}$  and  $\text{HOOI}$  for short, where  $\text{AM}(\widehat{K})$  is based on an estimated number of adaptively merged intervals and  $\text{ES}(L)$  is a slightly modified version of Poisson tensor PCA built on  $L$  equally spaced intervals. Their numeric performance is assessed by the average tensor

estimation error based on the corresponding intervals.

**Example 1.** The dataset is generated based on the temporal network embedding model, where the ranks are set as  $r_1 = r_2 = r_3 = 2$ . The columns of  $\mathbf{U}^*/\sqrt{n_1}$  and  $\mathbf{V}^*/\sqrt{n_2}$  are generated uniformly from  $\mathbb{O}_{n,2}$ , while the columns of  $\mathbf{W}_\eta^*$  are randomly generated such that  $\int_0^T \mathbf{w}^*(t)\mathbf{w}^*(t)^\top dt = T\mathbf{I}_2$ . For  $\mathcal{S}^*$ , the diagonal entries are set to be 0.5 and the rest entries 0.

**Example 2.** The dataset is generated based on the dynamic stochastic co-block model, where the block membership remains the same within each time interval but changes from one interval to the next. Specifically, let  $(\mathcal{M}_\eta^*)_{[.,k]} = \mathbf{Z}_k \mathbf{B} (\mathbf{X}_k)^\top$ , where  $\mathbf{Z}_k \in \{0, 1\}^{n_1 \times d}$ ,  $\mathbf{X}_k \in \{0, 1\}^{n_2 \times d}$  and  $\mathbf{B} \in (0, 1)^{d \times d}$ . Here, each row of  $\mathbf{Z}_k$  and  $\mathbf{X}_k$  has exact one 1, representing the block membership for nodes in  $\mathcal{N}_1$  and  $\mathcal{N}_2$ . Let  $\psi_{ik} \in [d]$  and  $\phi_{jk} \in [d]$  denote the membership for the  $i$ -th node in  $\mathcal{N}_1$  and the  $j$ -th node in  $\mathcal{N}_2$  within the time interval  $[\eta_{k-1}, \eta_k]$ . We generate  $\psi_{ik}$  and  $\phi_{jk}$  uniformly from  $[d]$ , and  $(\mathbf{B})_{ij}$  uniformly from  $[-0.5, 0.5]$ , where  $d$  is set to be 3.

In both examples, we let  $T$  take value in  $\{300, 400, 500\}$ , and  $n_1 = n_2 = n \in \{50, 100\}$ . We set  $\lambda_0 = 0.05$ ,  $K = T/100$ , and the partition  $\eta \in \mathbb{R}^K$  is constructed in a way such that each  $\eta_k$  is randomly generated from  $[0, T)$ , where the length ratio for the largest and smallest intervals is no larger than 3. For the proposed method, we initialize it with  $ES(L)$  with  $L = 100K$  on equally spaced intervals, and obtain the final estimate  $AM(\widehat{K})$  based on the adaptively merged intervals. In addition, we also apply HOSVD and HOOI on  $\log((\mathcal{Y}_\delta + 1/2)/(\lambda_0 \Delta_\delta))$  based on the equally spaced intervals (Han et al., 2022), where  $(\mathcal{Y}_\delta)_{ijl} = |\mathcal{T}_{ij} \cap [\delta_{l-1}, \delta_l]|$ . The averaged tensor estimation errors over 50 independent replications and their standard errors for each method are summarized in Tables 1 and 2.

It is evident that  $AM(\widehat{K})$  has delivered superior numerical performance and outperforms the other three competitors in all scenarios of both examples, showing that adaptively merged intervals indeed lead to substantial advantage in terms of estimation. It is also interesting to

Table 1: The averaged tensor estimation errors and their standard errors (in parentheses) for various methods over 50 independent replications in Example 1. All numbers are multiplied by 100.

|           | Method          | $T = 300$             | $T = 400$             | $T = 500$             |
|-----------|-----------------|-----------------------|-----------------------|-----------------------|
| $n = 50$  | AM( $\hat{K}$ ) | <b>0.3755</b> (0.039) | <b>0.2725</b> (0.032) | <b>0.2524</b> (0.035) |
|           | ES( $L$ )       | 1.064(0.065)          | 1.124 (0.055)         | 1.002(0.052)          |
|           | HOSVD           | 610.2(0.139)          | 609.2(0.111)          | 610.1(0.119)          |
|           | HOOI            | 610(0.127)            | 608.8(0.105)          | 6.089(0.001)          |
| $n = 100$ | AM( $\hat{K}$ ) | <b>0.2043</b> (0.017) | <b>0.1523</b> (0.013) | <b>0.1154</b> (0.008) |
|           | ES( $L$ )       | 0.35 (0.024)          | 0.3109(0.015)         | 0.5604(0.020)         |
|           | HOSVD           | 606 (0.060)           | 608.5(0.062)          | 610.3(0.052)          |
|           | HOOI            | 606.1(0.065)          | 608.2(0.059)          | 609.6(0.050)          |

Table 2: The averaged tensor estimation errors and their standard errors (in parentheses) for various methods over 50 independent replications in Example 2. All numbers are multiplied by 100.

|           | Method          | $T = 300$            | $T = 400$            | $T = 500$            |
|-----------|-----------------|----------------------|----------------------|----------------------|
| $n = 50$  | AM( $\hat{K}$ ) | <b>3.708</b> (0.289) | <b>4.357</b> (0.253) | <b>4.909</b> (0.211) |
|           | ES( $L$ )       | 5.938(0.836)         | 7.521 (1.179)        | 10.15(1.133)         |
|           | HOSVD           | 574.5(0.131)         | 571.4(0.092)         | 573.7(0.096)         |
|           | HOOI            | 574.2(0.130)         | 571.1(0.104)         | 573.4(0.093)         |
| $n = 100$ | AM( $\hat{K}$ ) | <b>1.5</b> (0.080)   | <b>1.624</b> (0.067) | <b>1.816</b> (0.077) |
|           | ES( $L$ )       | 1.528 (0.165)        | 1.787(0.259)         | 2.117(0.269)         |
|           | HOSVD           | 571.1(0.065)         | 562.8(0.059)         | 568.7(0.052)         |
|           | HOOI            | 570.6(0.064)         | 562.4(0.069)         | 568.3(0.056)         |

remark that ES( $L$ ) shows great advantage over HOSVD and HOOI, suggesting superiority of likelihood-based methods in temporal network estimation.

We now scrutinize how the tensor estimation error, as well as the embedding error, is affected by different choices of  $L$  in Example 1 with  $n = 50$ ,  $T = 400$  and  $K = 4$ . The left panel of Figure 1 shows the average tensor estimation errors of ES( $L$ ) over 50 independent replications with different  $L$ . Clearly, as  $L$  increases, the error dramatically decreases at



first, and then slowly increases. This is because the bias induced by the partition with a small number of intervals dominates the tensor estimation error in each interval, which will be reduced dramatically as  $L$  increases. Yet, as  $L$  becomes larger, the estimation variance begins to dominate the tensor estimation error, and it increases along with  $L$ . This phenomenon validates the asymptotic upper bound in Theorem 1. The averaged tensor estimation error of  $\text{AM}(\widehat{K})$  with  $\widehat{K} = 4$  adaptively merged intervals is represented by the red dotted line, which is substantially smaller than that of all the methods based on equally spaced intervals, demonstrating the advantage of the proposed methods in Theorem 3. Furthermore, it is also noted that similar U-pattern can be observed for the embedding error for both  $\mathbf{U}$  and  $\mathbf{V}$ , as showed in the middle and right panels of Figure 1, which validates results of Corollary 1.

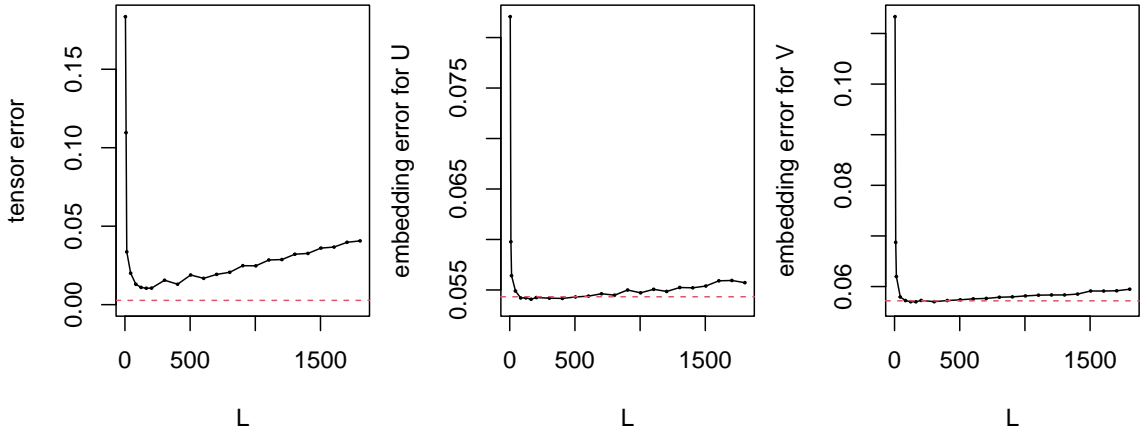


Figure 1: The three panels respectively show the average tensor estimation errors, embedding errors for  $\mathbf{U}$  and embedding errors for  $\mathbf{V}$  of the estimate based on equal spaced intervals with different values of  $L$  over 50 independent replications. The red dotted lines are the average estimation errors of the estimate based on adaptively merged intervals.

## 5.2 Real example

We apply the proposed method to analyze a temporal network based on the militarized interstate dispute dataset (Palmer et al., 2022). The dataset consists of all the major interstate disputes and involved countries during 1895-2014. It can be converted into a temporal network with  $\mathcal{N}_1 = \mathcal{N}_2$  containing all countries ever involved in any dispute over the years. Particularly, we set  $dy_{ij}(t) = 1$  if country  $i$  cooperated with country  $j$  in a militarized interstate dispute occurred at time  $t$ . We keep it as 1 for the following years until a dispute occurred between themselves, and then  $dy_{ij}(t)$  changes to 0 and remains until the next cooperation. This pre-processing step leads to a temporal network with  $n_1 = n_2 = 195$  nodes and 110066 temporal edges, and the time stamps range from 0 to  $T = 120$  years. We apply the proposed method with  $\Delta_\delta = 5$  years and thus  $L = 24$ , where the ranks are set to be  $(r_1, r_2, r_3) = (2, 2, 2)$  following a similar rank selection procedure in Han et al. (2022).

To assess the numeric performance, we randomly split the node pairs into 5 disjoint subsets  $\{\mathcal{P}_p\}_{p=1}^5$ . For each  $p$ , we obtain the estimated tensor  $\widehat{\mathcal{M}}^{(p)}$  on  $\mathcal{P}_{-p} = [n_1] \times [n_2] \setminus \mathcal{P}_p$ , and validate the estimation accuracy on  $\mathcal{P}_p$ ,

$$\text{err}^{(p)} = \frac{\|(\mathcal{T} - \widehat{\mathcal{Y}}^{(p)}) \circ \mathbf{1}_{\mathcal{P}_p}\|_F}{\|\mathcal{T} \circ \mathbf{1}_{\mathcal{P}_p}\|_F},$$

where  $\mathcal{T} = (\mathcal{T}_{ij})_{n_1 \times n_2}$  and  $\widehat{\mathcal{Y}}^{(p)} \in \mathbb{R}^{n_1 \times n_2}$  contain the true and estimated numbers of temporal edges for each node pair  $(i, j)$ ,  $\mathbf{1}_{\mathcal{P}_p} \in \mathbb{R}^{n_1 \times n_2}$  is the indicator matrix for  $\mathcal{P}_p$ , and  $\circ$  denotes the matrix Hadamard product. Then, the testing error is calculated as  $\text{err} = \sum_{p=1}^5 \text{err}^{(p)} / 5$ . For  $\text{AM}(\widehat{K})$ ,  $\widehat{\mathcal{Y}}_{\widehat{\boldsymbol{\eta}}}^{(p)}$  is obtained by  $(\widehat{\mathcal{Y}}_{\widehat{\boldsymbol{\eta}}}^{(p)})_{ij} = \sum_{k=1}^{\widehat{K}} \lambda_0 \exp((\widehat{\mathcal{M}}_{\widehat{\boldsymbol{\eta}}}^{(p)})_{ijk})(\widehat{\eta}_k - \widehat{\eta}_{k-1})$ , whereas  $(\widehat{\mathcal{Y}}_{\delta}^{(p)})_{ij} = \sum_{l=1}^{\widehat{L}} \lambda_0 \exp((\widehat{\mathcal{M}}_{\delta}^{(p)})_{ijk})(\delta_l - \delta_{l-1})$  for  $\text{ES}(L)$ . The estimates by HOSVD and HOOI are obtained in the same way as in Section 5.1. The averaged testing errors and their standard errors for the competing methods over 50 times replications are provided in Table 3, supporting the advantage of adaptively merged intervals in  $\text{AM}(\widehat{K})$  over the other three

competitors.

Table 3: The average testing errors and standard errors (in parentheses) for various methods over 50 replications.

| AM( $\hat{K}$ )      | ES(L)        | HOSVD        | HOOI         |
|----------------------|--------------|--------------|--------------|
| <b>0.739</b> (0.037) | 0.752(0.087) | 1.160(0.002) | 1.163(0.002) |

Furthermore, the output of AM( $\hat{K}$ ) yields that  $\hat{K} = 6$  and  $\hat{\boldsymbol{\eta}} = (20, 45, 50, 95, 105, 120)$ , and thus the adaptively merged time intervals are 1895-1914, 1915-1939, 1940-1944, 1945-1989, 1990-1999 and 2000-2014. These intervals appear to be closely related with a number of major world-wide events: before WWI, recess between WWI and WWII, WWII, Cold War, the 90s, and the 21st century. The estimated temporal embedding vectors  $\{\hat{\mathbf{w}}_{l,\delta}\}_{l=1}^L$  are shown in Figure 2, where  $\hat{\mathbf{w}}_{l,\delta}$  in different merged time intervals, represented by different colors, are well separated.

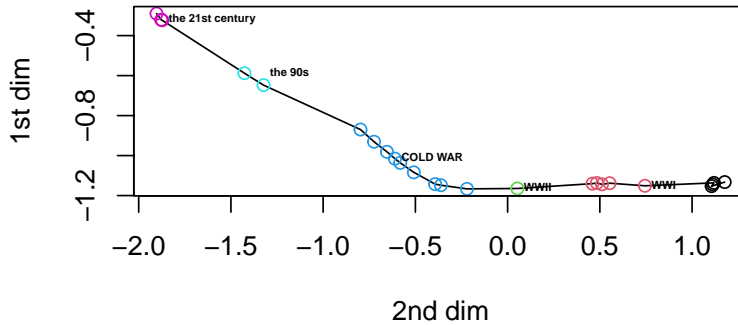


Figure 2: The estimated temporal embedding vectors  $\{\hat{\mathbf{w}}_{l,\delta}\}_{l=1}^9$ , where colors represent different merged time intervals.

## Acknowledgment

This research is supported in part by HK RGC Grants GRF-11304520, GRF-11301521, and GRF-11311022.

## References

- Aggarwal, C. and Subbian, K. (2014). Evolutionary network analysis: A survey. *ACM Computing Surveys (CSUR)*, 47:1–36.
- Avena-Koenigsberger, A., Misic, B., and Sporns, O. (2018). Communication dynamics in complex brain networks. *Nature reviews neuroscience*, 19:17–33.
- Cai, J.-F., Li, J., and Xia, D. (in press, 2022). Generalized low-rank plus sparse tensor estimation by fast riemannian optimization. *Journal of the American Statistical Association*.
- Cranmer, S. J. and Desmarais, B. A. (2011). Inferential network analysis with exponential random graph models. *Political analysis*, 19:66–86.
- De Lathauwer, L., De Moor, B., and Vandewalle, J. (2000a). A multilinear singular value decomposition. *SIAM journal on Matrix Analysis and Applications*, 21:1253–1278.
- De Lathauwer, L., De Moor, B., and Vandewalle, J. (2000b). On the best rank-1 and rank- $(r_1, r_2, \dots, r_n)$  approximation of higher-order tensors. *SIAM journal on Matrix Analysis and Applications*, 21:1324–1342.
- De Ruiter, P. C., Wolters, V., and Moore, J. C. (2005). *Dynamic food webs: multispecies assemblages, ecosystem development and environmental change*. Elsevier.
- Han, R., Willett, R., and Zhang, A. R. (2022). An optimal statistical and computational framework for generalized tensor estimation. *The Annals of Statistics*, 50:1–29.

- Hanneke, S., Fu, W., and Xing, E. P. (2010). Discrete temporal models of social networks. *Electronic journal of statistics*, 4:585–605.
- Hao, N., Niu, Y. S., and Zhang, H. (2013). Multiple change-point detection via a screening and ranking algorithm. *Statistica Sinica*, 23:1553.
- Hays, J. C., Kachi, A., and Franzese Jr, R. J. (2010). A spatial model incorporating dynamic, endogenous network interdependence: A political science application. *Statistical Methodology*, 7:406–428.
- Hoff, P., Raftery, A., and Handcock, M. (2002). Latent space approaches to social network analysis. *Journal of the American Statistical Association*, 97:1090–1098.
- Holme, P. and Saramäki, J. (2012). Temporal networks. *Physics reports*, 519:97–125.
- Huang, S., Weng, H., and Feng, Y. (in press, 2022). Spectral clustering via adaptive layer aggregation for multi-layer networks. *Journal of Computational and Graphical Statistics*.
- Kim, B., Lee, K. H., Xue, L., and Niu, X. (2018). A review of dynamic network models with latent variables. *Statistics surveys*, 12:105.
- Kinne, B. J. (2013). Network dynamics and the evolution of international cooperation. *American Political Science Review*, 107:766–785.
- Lyu, Z., Xia, D., and Zhang, Y. (2021). Latent space model for higher-order networks and generalized tensor decomposition. *arXiv preprint arXiv:2106.16042*.
- Matias, C. and Miele, V. (2017). Statistical clustering of temporal networks through a dynamic stochastic block model. *Journal of the Royal Statistical Society: Series B (Statistical Methodology)*, 79:1119–1141.

- Niu, Y. S., Hao, N., and Zhang, H. (2016). Multiple change-point detection: A selective overview. *Statistical Science*, 31:611–623.
- Palmer, G., McManus, R. W., D’Orazio, V., Kenwick, M. R., Karstens, M., Bloch, C., Dietrich, N., Kahn, K., Ritter, K., and Soules, M. J. (2022). The mid5 dataset, 2011–2014: Procedures, coding rules, and description. *Conflict Management and Peace Science*, 39:470–482.
- Perry, P. O. and Wolfe, P. J. (2013). Point process modelling for directed interaction networks. *Journal of the Royal Statistical Society: Series B (Statistical Methodology)*, 75:821–849.
- Perry-Smith, J. E. and Shalley, C. E. (2003). The social side of creativity: A static and dynamic social network perspective. *Academy of management review*, 28:89–106.
- Sewell, D. K. and Chen, Y. (2015). Latent space models for dynamic networks. *Journal of the American Statistical Association*, 110:1646–1657.
- Sewell, D. K. and Chen, Y. (2016). Latent space models for dynamic networks with weighted edges. *Social Networks*, 44:105–116.
- Sit, T., Ying, Z., and Yu, Y. (2021). Event history analysis of dynamic networks. *Biometrika*, 108:223–230.
- Snijders, T. A. (2001). The statistical evaluation of social network dynamics. *Sociological methodology*, 31:361–395.
- Snijders, T. A. (2017). Stochastic actor-oriented models for network dynamics. *Annual review of statistics and its application*, 4:343–363.
- Snijders, T. A., Koskinen, J., and Schweinberger, M. (2010). Maximum likelihood estimation for social network dynamics. *The annals of applied statistics*, 4:567.

- Sporns, O., Chialvo, D. R., Kaiser, M., and Hilgetag, C. C. (2004). Organization, development and function of complex brain networks. *Trends in cognitive sciences*, 8:418–425.
- Ulanowicz, R. E. (2004). Quantitative methods for ecological network analysis. *Computational biology and chemistry*, 28:321–339.
- Voytek, B. and Knight, R. T. (2015). Dynamic network communication as a unifying neural basis for cognition, development, aging, and disease. *Biological psychiatry*, 77:1089–1097.
- Vu, D., Hunter, D., Smyth, P., and Asuncion, A. (2011a). Continuous-time regression models for longitudinal networks. In Shawe-Taylor, J., Zemel, R., Bartlett, P., Pereira, F., and Weinberger, K., editors, *Advances in Neural Information Processing Systems*, volume 24. Curran Associates, Inc.
- Vu, D. Q., Asuncion, A. U., Hunter, D. R., and Smyth, P. (2011b). Dynamic egocentric models for citation networks. In *International Conference on Machine Learning*, page 857–864.
- Yu, Y., Wang, T., and Samworth, R. J. (2015). A useful variant of the davis–kahan theorem for statisticians. *Biometrika*, 102:315–323.
- Zhang, J., He, X., and Wang, J. (in press, 2022). Directed community detection with network embedding. *Journal of the American Statistical Association*.
- Zhen, Y. and Wang, J. (in press, 2022). Community detection in general hypergraph via graph embedding. *Journal of the American Statistical Association*.